FULL PAPER

Dalton
www.rsc.org/dalton

# The preparation and characterisation of cyclam/anthraquinone macrocyle/intercalator complexes and their interactions with DNA †

**Leanne T. Ellis,[a] David F. Perkins,[b] Peter Turner[a] and Trevor W. Hambley *[a]**

[a] *Centre for Heavy Metals Research, School of Chemistry, University of Sydney, NSW 2006, Australia. E-mail: t.hambley@chem.usyd.edu.au*

[b] *Institute for Biomolecular Sciences, University of Wollongong, Wollongong, NSW 2522, Australia*

***Received 24th February 2003, Accepted 21st May 2003***
***First published as an Advance Article on the web 5th June 2003***

A new series of macrocycle/intercalator adducts have been prepared from cyclam (1,4,8,11-tetraazacyclotetradecane) and the 1- and 2-substituted anthraquinones (1-[(2-aminoethyl)amino]anthracene-9,10-dione (1C2mac), 1-[(3-aminopropyl)amino]anthracene-9,10-dione (1C3mac), 2-[(3-aminopropyl)amino]anthracene-9,10-dione (2C3mac)). The copper complexes of two of these adducts were prepared and the crystal structure of the complex of 1C2mac ($[Cu(1C2mac)(CH_3CN)_2](PF_6)_2.0.2H_2O$) was determined as the hexafluorophosphate salt. The equilibrium constants for the binding to DNA of 1C2-mac, with and without the copper added, were found by UV titrations to be $4.7 \times 10^3$ $M^{-1}$ and $6.2 \times 10^3$ $M^{-1}$, respectively. Reaction with plasmid DNA allowed comparison between the effects of the cyclam/anthraquinone adducts, their copper complexes and the intercalators alone. Addition of the macrocycle increased the extent and effect of DNA intercalation and addition of copper increased the effect still further. The adducts with the longer side chains caused substantially more unwinding of the DNA. None of the adducts inhibited cleavage at dGpG or dGpC sites by restriction enzymes. Molecular modelling was used to investigate the effects of the side chain for a number of possible DNA binding modes. These models reveal that intercalation is not significantly interfered with by the presence of the macrocycle, irrespective of the position of attachment. The increased unwinding caused by adducts with the longer side chain is therefore most likely to be due to specific interactions between the macrocycle and the DNA.

## Introduction

The localisation of macrocyclic metal complexes on DNA is of interest for a number of reasons. If the metal ion is a radionuclide, increased DNA damage will result,[1] if it is a metal that facilitates phosphate hydrolysis, then DNA cleavage may result [2] and if the metal binds to DNA bases, then sequence selective binding can occur.[3] Intercalators bind rapidly and reversibly to DNA and have been shown to increase the rate and extent of DNA binding of a variety of groups including metal complexes.[3–6] Kimura and colleagues have described a series of macrocyclic complexes linked to intercalators and have shown that these interact in a sequence selective manner with DNA.[3,7–12] They have also shown that the sequence selectivity depends on the metal ion, the nature of the intercalator and the nature and position of the link between the macrocycle and the intercalator.[3,7–12] In all of these studies the macrocycle employed was the 12-membered ring, cyclen (1,4,7,10-tetraazacyclododecane), a ligand that forces the metal to lie out of the coordination plane promoting interactions with the DNA.

The 14-membered tetraazamacrocycle cyclam (1,4,8,11-tetraazacyclotetradecane) can tightly bind a wide range of metal ions including radionuclides, phosphate-hydrolysis-promoting metal ions and metals that can bind to DNA. Therefore, we were interested in attaching cyclam to an intercalator and establishing how this influenced interactions with DNA. Here we describe the preparation of a series of cyclam/anthraquinone adducts (Scheme 1), the copper(II) complexes of two of these and experimental and molecular mechanics modelling studies of the interactions between the adducts and DNA.

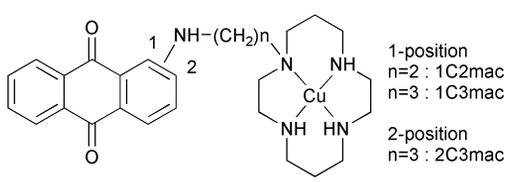


**Scheme 1**

## Experimental

### Instrumentation

Mass spectra were obtained in the appropriate solvents (flow rate 100 μL per minute) on a Finnigan LCQ MS Detector and presented as an electrospray ionisation low resolution mass spectrum using Finnigan LCQ data processing software (version 12.0). An ESI spray voltage of 4 kV was applied and a nitrogen sheath gas pressure of 60 psi with a heated capillary temperature of 200 °C were used. Diffuse reflectance infrared transform spectra (DRIFTS) were recorded in a potassium bromide background on a Bio-Rad FTS-40 spectrometer using Win-IR software. $^1$H NMR spectra were collected on a Bruker AC200F 200 MHz spectrometer and referenced to TMS or solvent used. $^{195}$Pt NMR spectroscopy was carried out by Jacques Nemorin of The University of Sydney on a Bruker Avance 600 MHz spectrometer, referenced externally to $K_2PtCl_4$ in $D_2O$ at −1624 ppm. Elemental analyses were carried out by Reet Bergman at the Microanalytical Unit of the Research School of Chemistry at the Australian National University, Canberra.

### 1-[(Hydroxyethyl)amino]anthracene-9,10-dione, 1C2OH

1-Chloroanthracene-9,10-dione (15 g, 63 mmol) was heated in butanol (150 mL). When the solution became clear yellow (at ~70 °C), ethan-1-ol-2-amine (15 mL, 0.255 mol) was added

† Electronic supplementary information (ESI) available: Figs. S1–8; gel electrophoresis patterns, $^1$H NMR spectra, and overlap interactions between the macrocycle and DNA. See http://www.rsc.org/suppdata/dt/b3/b302123h/

DOI: 10.1039/b302123h

quickly and the solution refluxed for 3 h. The solution went from yellow to deep red, was cooled to room temperature and concentrated to about 60 mL. The reaction mixture was allowed to cool to room temperature and then cooled to −20 °C overnight. The solid product was removed by filtration, recrystallised from ethyl acetate and then column chromatographed (silica gel 60, particle size 0.040–0.063 nm, 3 × 25 cm). Impurities were eluted with petroleum ether–ethyl acetate (1 : 2), then chloroform–ethanol (9 : 1) was added to elute the pure red product. The solvent was removed by rotary evaporation and the red solid placed in an oven to dry (100 °C) (yield 75%). The NMR spectrum ($CDCl_3$) was in accord with the proposed structure.

### 1-[2-(Bromoethyl)amino]anthracene-9,10-dione, 1C2Br

1C2OH (0.85 g, 3.2 mmol) was dissolved in dry dichloromethane (45 mL) and 1 equivalent of dry pyridine (111 μL) was added. The solution was heated to 40 °C, 1 equivalent of thionyl bromide (257 μL) was added and the solution was refluxed for 5 h. Progress of the reaction was monitored by TLC (silica gel, $CHCl_3$) and an extra 50 μL of thionyl bromide was added twice to drive it to completion. The reaction mixture was then cooled to room temperature and water was carefully added to decompose and remove excess thionyl bromide. The organic phase was washed with water twice and dried with magnesium sulfate, filtered and rotary evaporated to dryness. The product was dissolved in minimal chloroform and loaded onto a silica gel column (4 × 40 cm) and eluted with chloroform. The first major band was collected, evaporated to dryness and dried in an oven at 110 °C for 2 h (yield 78%). The NMR spectrum ($CHCl_3$) was in accord with the proposed structure.

### 2-[(Hydroxypropyl)amino]anthracene-9,10-dione, 2C3OH

2-Chloroanthracene-9,10-dione (5 g, 21 mmol) and propan-1-ol-3-amine (10 mL, excess) were refluxed in butanol (50 mL) under nitrogen overnight. The reaction was monitored by TLC (silica gel, chloroform). The reaction mixture was cooled to room temperature and then cooled to −20 °C overnight, filtered and the solid obtained was recrystallised from ethyl acetate. The product was column chromatographed (silica gel 60, particle size 0.040–0.063 nm, 3 × 35 cm) with chloroform as the eluent until the desired product started eluting. The product was then eluted with 50 : 50 chloroform–ethanol. The solvent was removed by rotary evaporation and the product dried in an oven at 110 °C (yield 35%). The NMR spectrum ($d_6$-DMF) was in accord with the proposed structure.

### 2-[3-(Bromopropyl)amino]anthracene-9,10-dione, 2C3Br

2C3OH (0.1 g, 35.6 mmol) was dissolved in dry dichloromethane (10 mL) and 1 equivalent of dry pyridine (29 μL) was added. The solution was heated to 40 °C, 1 equivalent of thionyl bromide (28 μL) was added and the solution was then refluxed for 5 h. Progress of the reaction was monitored by TLC (silica gel, chloroform) and an extra 10 μL of thionyl bromide was added twice to drive it to completion. The reaction mixture was then cooled to room temperature and water was carefully added to decompose and remove excess thionyl bromide. The organic phase was washed with water twice and dried with magnesium sulfate, filtered and rotary evaporated to dryness. The product was dissolved in minimal chloroform and loaded onto a silica gel column (1.5 × 20 cm) and eluted with chloroform. The first major band was collected, evaporated to dryness and dried in an oven at 110 °C for 1 h (yield 41%). The NMR spectrum ($CHCl_3$) was in accord with the proposed structure.

### Macrocycle/intercalator syntheses

**General procedure.** 1,4,8,11-Tetraazacyclotetradecane (cyclam, 5 equivalents, Sigma-Aldrich) was dissolved in hot toluene (10 mL), the appropriate brominated anthraquinone (1 equivalent), $Cs_2CO_3$ (1 equivalent) and a catalytic amount of KI were added and the reaction mixture was refluxed for 2 h. The reactions were monitored by TLC (silica gel, $CHCl_3$). The reaction mixture was cooled to room temperature and the excess cyclam that precipitated was filtered off. The filtrate was washed with aqueous sodium hydroxide (5%, 3 × 5 mL), water (2 × 5 mL) and dried with magnesium sulfate. The solution was rotary evaporated to dryness and the yellow solid collected. The solid was dissolved in chloroform and column chromatographed on silica gel 60 (particle size 0.040–0.063 nm, 4 × 20 cm, $CHCl_3$–EtOH–$NH_4OH$, 70 : 25 : 5). The last band eluted was the desired product.

**2Cmac:** cyclam (0.5 g, $2.5 \times 10^{-4}$ mol), 2-bromomethylanthracene-9,10-dione (0.015 g, $5 \times 10^{-5}$ mol, Sigma-Aldrich), yield 72%. MS (EI): 421, [M + $H^+$]. The NMR spectrum is in accord with the proposed structure, (ESI,† Fig. S3). $C_{25}H_{32}N_4O_2$; found: C, 71.0; H, 7.4; N, 12.9%; calc.: C, 71.4; H, 7.7; N 13.3%.

**1C2mac:** cyclam (0.254 g, $1.3 \times 10^{-3}$ mol), 1C2Br (0.084 g, $2.54 \times 10^{-5}$ mol), yield 87%. MS (EI): 450.3, [M + $H^+$]. The NMR spectrum is in accord with the proposed structure (ESI,† Fig. S4). $C_{26}H_{37}N_5O_2^{2+}$, $2HCO_3^-.2H_2O$; MW 609.6, found: C, 53.4; H, 6.8; N, 11.3%; calc.: C, 55.2; H, 7.1; N 11.4%.

**1C3mac:** cyclam (0.254 g, $1.3 \times 10^{-3}$ mol), 1C3Br (0.088 g, $2.54 \times 10^{-5}$ mol), yield 37%, MS (EI): 464.4, [M + $H^+$]. The NMR spectrum is in accord with the proposed structure. $C_{27}H_{39}N_5O_2^{2+}$, $2HCO_3^-.2H_2O$; MW 623.7, found: C, 57.8; H, 6.9; N, 11.2%; calc.: C, 55.8; H, 7.3; N, 11.2%.

**2C3mac:** cyclam (0.058 g, $3.0 \times 10^{-4}$ mol), 2C3Br (0.020 g, $5.8 \times 10^{-5}$ mol), yield 63%, MS (EI): 464.4 [M + $H^+$].

### Syntheses of copper complexes

**General procedure.** The appropriate cyclam/anthraquinone (16.0 mmol) was dissolved in a minimum of dimethylformamide and water (~10 mL) was added. Copper(II) acetate was dissolved in the minimum amount of water and added to the solution. The pH was checked and if necessary was adjusted to be 5.5 with either hydrochloric acid (1 M) or sodium hydroxide (1 M). The reaction was allowed to proceed at room temperature and monitored by TLC (silica gel, $CHCl_3$–EtOH–$NH_3$, 70 : 25 : 5). Further aliquots of copper acetate were added every hour until the spot due to the starting material disappeared. Dichloromethane was added to the reaction mixture followed by a saturated solution of sodium hexafluorophosphate resulting in movement of the red product into the dichloromethane layer. The organic layer was washed twice with water (with a few drops of saturated sodium hexafluorophosphate added to the water layer if necessary to keep the red product in the dichloromethane layer). The solvent was removed by rotary evaporation and TLC (silica gel, $CHCl_3$–EtOH–$NH_3$ 70 : 25 : 5) showed only a clean spot on the baseline. The solid was dissolved in acetonitrile and isopropyl ether was diffused into a refrigerated solution to purify the product and to obtain X-ray quality crystals.

**Cu–2Cmac:** yield 27%. MS (EI): 482.1 [M +$H^+$], 241.7 [2+ charge]. [Cu(2Cmac)]$(PF_6)_2$, $CuC_{25}H_{32}N_4O_2(PF_6)_2$; MW 774.1, found: C, 38.3; H, 4.6; N, 7.3%; calc.: C, 38.8; H, 4.2; N, 7.2%.

**Cu–1C2mac:** yield 39%. MS (EI): 511.2, [M +$H^+$], 256 [2+ charge]. [Cu(1C2mac)$(CH_3CN)_2$]$(PF_6)_2 \cdot 0.2H_2O$, $CuC_{30}H_{41}N_7O_2(PF_6)_2 \cdot 2CH_3CN$; MW 885.2, found: C, 40.54; H, 4.78; N, 10.99%; calc.: C, 40.70; H, 4.67; N, 11.07%.

### X-Ray crystallography

Crystals obtained by the vapour diffusion of isopropyl ether into an acetonitrile solution of the Cu–1C2mac complex initially formed too quickly, so toluene was added to the isopropyl ether and the solution refrigerated to slow the crystal formation and produce higher quality crystals. A crystal was

attached to a thin glass fibre and mounted on a Bruker SMART 1000 CCD diffractometer employing graphite-monochromated Mo-Kα radiation generated from a sealed tube. Cell constants at 150 °C were obtained from least-squares refinement against 5864 reflections located in a $2\theta$ range of 2.39 to 28.00°. Data were collected to 28.00° and the full sphere coverage was >99%. An empirical absorption correction, determined with SADABS,[13] was applied to the data and the data integration and reduction were undertaken with SAINT and XPREP.[14] The structure was solved by direct methods with SHELXS-86,[15] and refined using teXsan.[16] Hydrogen atoms were included at calculated sites and non-hydrogen atoms were refined anisotropically. The two contributors to the disordered anthraquinone moiety were each refined with a 50% occupancy. Neutral atom scattering factors were taken from International Tables.[17] Anomalous dispersion effects were included in $F_c$;[18] the values for $\Delta f'$ and $\Delta f''$ were those of Creagh and McAuley.[19] The values for the mass attenuation coefficients are those of Creagh and Hubbell.[20] All other calculations were performed using the teXsan crystallographic software package of Molecular Structure Corporation.[16] ORTEP[21] plots (30% thermal ellipsoids) of the complex are shown in Fig. 1(a) and (b).

**Crystal data for Cu–1C2mac.** Formula $CuC_{30}H_{42}N_7O_{2.2}P_2F_{12}$; $M_r = 888.12$, triclinic, space group $P\bar{1}$, $a = 8.304(2)$, $b = 9.899(3)$, $c = 22.647(6)$ Å, $\alpha = 95.644(5)$, $\beta = 95.614(4)$, $\gamma = 105.800(4)°$, $V = 1767.5(7)$ Å$^3$, $D_c = 1.669$ g cm$^{-3}$, $Z = 2$, $\mu$(Mo-Kα) = 0.814 mm$^{-1}$, $\lambda$(Mo-Kα) = 0.71063 Å, $T = 150$ K, $F(000) = 912$ electrons, $2\theta_{max} = 28.32$, $N = 8116$, $N_o = 5864$ ($I \geq 2.5\sigma(I)$), $N_{var} = 660$, max. shift = $0.08\sigma$, $R$ [$\Sigma(||F_o| - |F_c||)/\Sigma|F_o|$] = 0.050, $R_w$ [$\Sigma(w^{1/2}||F_o| - |F_c||)/\Sigma w^{1/2}|F_o|$] = 0.037 and $w = 1/\sigma^2$, $\rho_{max,min} = 0.50$, $-0.54$ e Å$^{-3}$.

CCDC reference number 204635.

See http://www.rsc.org/suppdata/dt/b3/b302123h/ for crystallographic data in CIF or other electronic format.

### UV Spectrophotometric titrations

UV spectroscopy was carried out on a HP 8452A Diode Array Spectrometer with HP 89531A MS-DOS-UV/VIS operating software. Stirring and temperature were controlled with a 8909A Peltier temperature control accessory. The spectrophotometric titration was performed using similar conditions to those used by Kikuta *et al.*[12] Salmon sperm DNA (Sigma) was dissolved in autoclaved, milli-Q $H_2O$ and filtered (MFS 13, cellulose acetate membrane, pore 0.02 μm, Millipore). The DNA concentration was determined spectrophotometrically, $\varepsilon_{260} = 6700$ M$^{-1}$ cm$^{-1}$ (per nucleotide).[22] Stock DNA was made up to a final concentration of 1 mM (nucleobases) in HEPES buffer (Sigma-Aldrich) (10 mM, pH 8.0, with $I = 0.1$ ($NaNO_3$)). The compounds (1C2mac and Cu–1C2mac, 20 μM) were made up in HEPES (10 mM, pH 8.0, with $I = 0.1$ ($NaNO_3$)). Stock DNA was added in increasing amounts (0–200 μM) to the cyclam/anthraquinone adduct or $Cu^{2+}$ complex (2 mL) in a 1 cm quartz cuvette with continuous stirring at 25 °C. The absorption at $\lambda_{max}$ was measured after each addition. The calculations for the binding constant were as described by Arounaguiri and Maiya[23] and Kikuta *et al.*[12]

### Plasmid binding

Plasmid binding experiments with DMF soluble compounds were adapted from methods described by Broomhead *et al.*[24] Fresh stocks of the water insoluble compounds (1 mg) were prepared by dissolving them in high purity DMF (2 mL) with sonication and slight warming if necessary. The solution was diluted with water (3 mL) and millipore filtered. Appropriate dilutions were made and the required volumes of solutions were added to the Eppendorf tubes to achieve a set of concentrations in the range 0–100 μM. Sterilised buffer (4 μL, 5 mM phosphate, pH 7.4), and PBR322 DNA (5 μL, 0.083 μg/μL $H_2O$) were added to each tube. The volume in each tube was adjusted to 20 μL with $H_2O$ and DMF to give a final solution with 20% DMF (v/v). The tubes were vortexed and pulse centrifuged to facilitate mixing and the reaction was allowed to proceed by incubation at 37 °C for 3 h. The samples were frozen to prevent any further reaction from taking place. A concentration range of 0–100 μM was used for the initial study of each compound and the results of these studies were then used to select the appropriate range.

Where relevant, a restriction enzyme and buffer were added. For *Bam*H1, X10 restriction buffer B (3 μL, 10 mM Tris-HCl, 5 mM $MgCl_2$, 100 mM NaCl, 1 mM 2-mercaptoethanol, pH 8.0, Roche Molecular Biochemicals) and *Bam*H1 (0.5 μL, activity 11 U/μL, excess, Roche Molecular Biochemicals) were added. For *Pvu*II, restriction buffer M (3 μL, 10 mM Tris-HCl, 10 mM $MgCl_2$, 50 mM NaCl, 1 mM dithioerythritol, pH 7.5, Roche Molecular Biochemicals) and *Pvu*II (0.5 μL, activity 10 U/μL, excess, Roche Molecular Biochemicals) were added. Water was added to give a final volume in each tube of 30 μL. The tubes were incubated at 37 °C for 1 h to allow any DNA digestion to take place, then rapidly cooled to 0 °C to prevent any further reaction from taking place.

Tracking dye (6 μL, 0.25% Bromophenol Blue, 40% sucrose in water) was added to each tube and 20 μL portions were loaded on an agarose gel and electrophoretically chromatographed. The agarose gels (Molecular biology certified agarose, ultra pure grade, BIO-RAD, made up to 1.5% w/v) were prepared using TBE buffer (90 mM Tris, 90 mM boric acid, 2 mM EDTA, adjusted to pH 8.0 with 10 M HCl) containing ethidium bromide (0.5 g mL$^{-1}$, Sigma). The agarose gel was immersed in TBE buffer solution with ethidium bromide (0.5 μg mL$^{-1}$). DNA size marker (1 μL in 5 μL tracking dye, λ DNA/*Hind*III digestion, Roche Molecular Biochemicals) was used as a standard and loaded onto the first lane of each gel. Electrophoresis was carried out at approximately 25 V for 18 h (Gene power supply GPS 200/400). For the post-staining experiments, the agarose gels were prepared in the same manner with the exclusion of the ethidium bromide in the agarose gel and TBE buffer. After the electrophoresis was complete, the gels were stained in TBE buffer (90 mM Tris, 90 mM boric acid, 2 mM EDTA, adjusted to pH 8.0 with 10 M HCl) containing ethidium bromide (0.5 mg mL$^{-1}$) for 2 h and then rinsed with water. Each gel was photographed under UV light through a clear and an orange filter (Wratten 2A and Wratten 22 Kodak filter) using Polaroid type 55 film (Foto Riesel). The photos were scanned with a Hewlett Packard ScanJet 6100C.

### Molecular modelling

The AMBER force field parameters were used for the nucleic acid interactions.[25] The models were constructed using the HyperChem programme.[26] The double stranded B-DNA (5′-CCCCGGGG-3′) was generated using the nucleic acid feature in the database of HyperChem and the intercalation site opened using distance constraints. The models were geometrically minimised using Fletcher-Reeves conjugate-gradient minimisation. Convergence was defined when the gradient of the average root mean square (RMS) shift reached 0.4 kJ Å$^{-1}$ mol$^{-1}$. Models that contained metals were set up in HyperChem without the metal present to produce a starting model, then transferred into the MOMEC-SG programme,[27] and minimised with the metal present. The calculations performed in MOMEC-SG used the Newton–Raphson method for energy minimisation.

## Results and discussion

### Macrocycle/intercalator syntheses

The procedure for the combination of the cyclam and the anthraquinone was adapted from a method for the addition of

naphthalene to cyclam reported by Engeser *et al.*[28] and involved the reaction between cyclam and an anthraquinone with a brominated side chain. Addition of $Cs_2CO_3$ and KI to catalyse the reaction was found to be necessary. Initially, the method was trialled using cyclam and 2-bromoanthraquinone and when this was shown to be successful, it was extended to alkylaminoanthraquinones with brominated side chains prepared using methods reported previously. The procedure is outlined in Scheme 2. Thus, 1C2OH and 2C3OH were prepared in a manner analogous to that described by Katzhendler *et al.*[29] for the preparation of 1C3OH. The preparation of 1C3Br has been reported by Gibson *et al.*[30] and the preparation of 1C2Br and 2C3Br by the same method was successful. These were used to prepare 1C2mac, 1C3mac and 2C3mac using the procedure described by Engeser *et al.*[28] Our attempts to complete the series by preparing 2C2mac were frustrated by the failure of all attempts to prepare the intermediate 2C2Br from 2C2OH despite numerous variations in the reaction conditions. There have been no other reports of 2C2Br in the literature and it may be that reaction of 2C2OH gives rise only to other products.

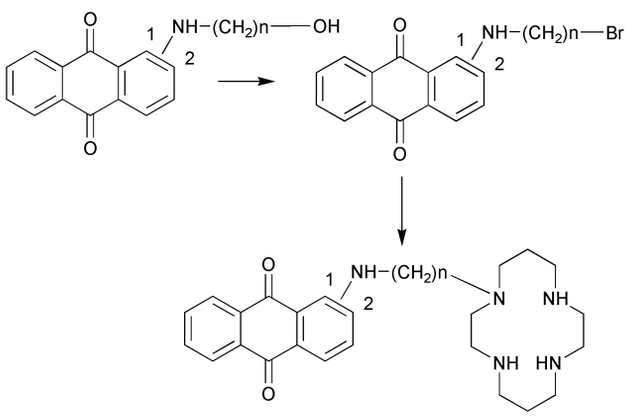


**Scheme 2**

### Syntheses of copper complexes

The procedure for the synthesis of the copper complexes of the cyclam/anthraquinones was adapted from that reported by Jones-Wilson *et al.*[25] and was tested using the C2mac complex. The cyclam/anthraquinone adducts were oily red products that were difficult to remove from the reaction flask. Therefore, chloroform was added to the entire sample and a portion was pipetted into another flask. The solvent was then removed and the amount transferred was weighed and used in the reaction. Formation of the copper complex was achieved by adding aliquots of copper(II) acetate until no trace of the free ligand was observable in a TLC. Purification of the complexes was readily achieved by diffusion of ether into an acetonitrile solution of the crude product.

### Crystal structure

The crystal structure of Cu–1C2mac confirms the synthesis of the desired product and ORTEP[21] plots (Fig. 1), show this product with two acetonitrile groups coordinated in the axial sites of the copper. There are two conformations of the adduct in the crystal lattice, with the anthraquinone in different orientations and with 50% occupancies (Fig. 1(a) and (b)). In both orientations, the rings of adjacent molecules in the lattice are stacked parallel to one another. The two orientations are approximately perpendicular to one another and atoms C(14), C(15), C(21) and C(22) of adjacent molecules overlap. This gives rise to anomalies in the bond lengths making detailed discussion of the geometry of the anthraquinone inappropriate. The copper–macrocycle moiety did not undergo this disorder. The interatomic distances and angles are similar to those from related structures of each of the two moieties. The average of

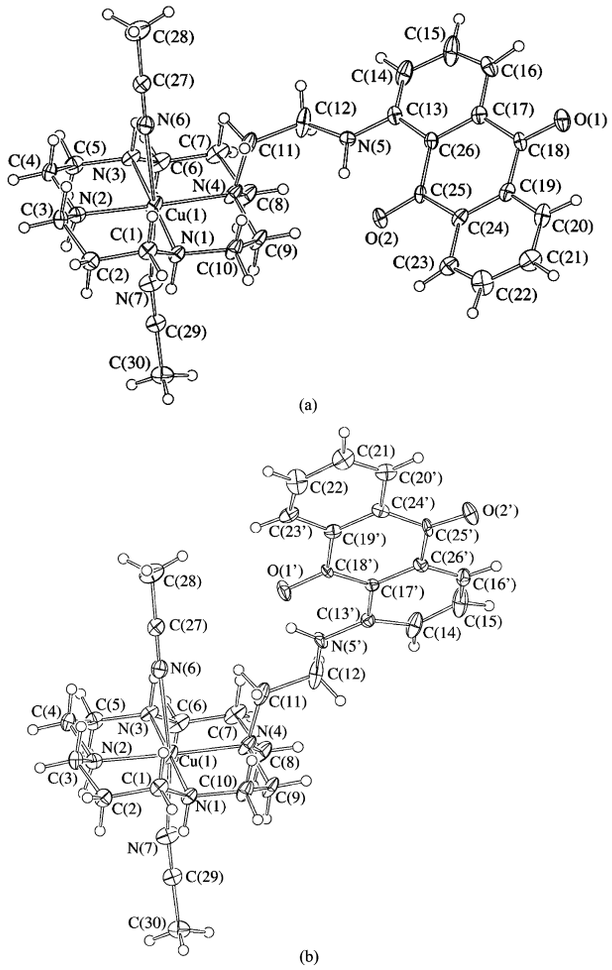


**Fig. 1** ORTEP plots for Cu–1C2mac, 30% probability ellipsoids.

the Cu–N(secondary amine) bond lengths is 2.014 Å, similar to the 2.021 Å in $[Cu(cyclam)(MeCN)_2]^{2+}$,[31] but the bond to the tertiary amine carrying the anthraquinone moiety is substantially longer at 2.061(3) Å. There is an intramolecular hydrogen bond between an oxygen atom of the anthraquinone and the hydrogen of the amine group in the side chain in both conformations of the Cu–1C2mac which is similar to that in the structure of a related anthraquinone moiety, 1-[2-(diethylamino)ethylamino)]anthraquinone.[32] There is a short contact (2.11 Å) between the H(C8) and H(N5) atoms of the anthraquinone moiety and the macrocycle moiety in one of the anthraquinone orientations (Fig. 1(a)), but no other significant interactions between the macrocyclic and intercalator groups are observed. The next shortest distances are 3.68 Å between O(2) and C(9) (Fig. 1(a)) and 3.55 Å between O(1′) and C(28) (Fig. 1(b)). Table 1 provides a comparisons of bond distances, angles and hydrogen bonds of Cu–1C2mac with other similar structures.

### UV spectrophotometric titrations

UV spectrophotometric titrations were carried out to compare the affinities of 1C2mac and its copper complex for salmon sperm DNA by determining their apparent binding constants ($K_{ap}$ ($M^{-1}$)). The observed decrease in the intensity of the absorption for each of the compounds on the addition of DNA was used to determine the binding constants using similar conditions to those described by Kikuta *et al.*[12]

The absorbance was measured at a maximum of 314 nm for 1C2mac (Fig. 2(a)) and 316 nm for Cu–1C2mac (Fig. 3(a)) over a range of salmon sperm DNA concentrations. There was a steady decrease in the intensity of the absorbance with the addition of each increment of salmon sperm DNA (0–200

**Table 1** Comparisons of bond distances, angles and hydrogen bonds of Cu–1C2mac with other similar structures

| | Cu–1C2mac | $[Cu(cyclam)(MeCN)_2]^{2+}$ [31] | 1-[2-(Diethylamino)ethylamino)]anthraquinone [32] |
|---|---|---|---|
| Cu–N(1) | 2.008(3) | 2.020(4) | |
| Cu–N(2) | 2.025(3) | 2.023(4) | |
| Cu–N(3) | 2.009(3) | | |
| Cu–N(4) | 2.061(3) | | |
| Cu–N(MeCN) | 2.485(3) | 2.575(5) | |
| Cu–N(MeCN) | 2.717(3) | | |
| N(1)–Cu–N(2) | 93.4(1) | 94.0(2) | |
| N(2)–Cu–N(3) | 86.1(1) | 86.0(2) | |
| N(3)–Cu–N(4) | 93.8(1) | | |
| N(4)–Cu–N(1) | 86.7(1) | | |
| N(1)–Cu–N(6) | 91.26(9) | 91.6(2) | |
| N(2)–Cu–N(6) | 82.89(9) | 87.3(2) | |
| N(3)–Cu–N(6) | 89.38(9) | | |
| N(4)–Cu–N(6) | 95.0(1) | | |
| N(1)–Cu–N(7) | 87.9(1) | 88.4(2) | |
| N(2)–Cu–N(7) | 90.0(1) | 92.7(2) | |
| N(3)–Cu–N(7) | 91.4(1) | | |
| N(4)–Cu–N(7) | 92.1(1) | | |
| H(N5) ··· O(2) | 1.823 | | 1.862(3) |
| N(5)–O(2) | 2.614 | | 2.638(3) |
| H(N5′) ··· O(1′) | 1.875 | | |
| N(5′)–O(1′) | 2.602 | | |

Distances are in angstroms (Å) and angles are in degrees (°). Estimated standard deviations in the least significant figure are given in parentheses.

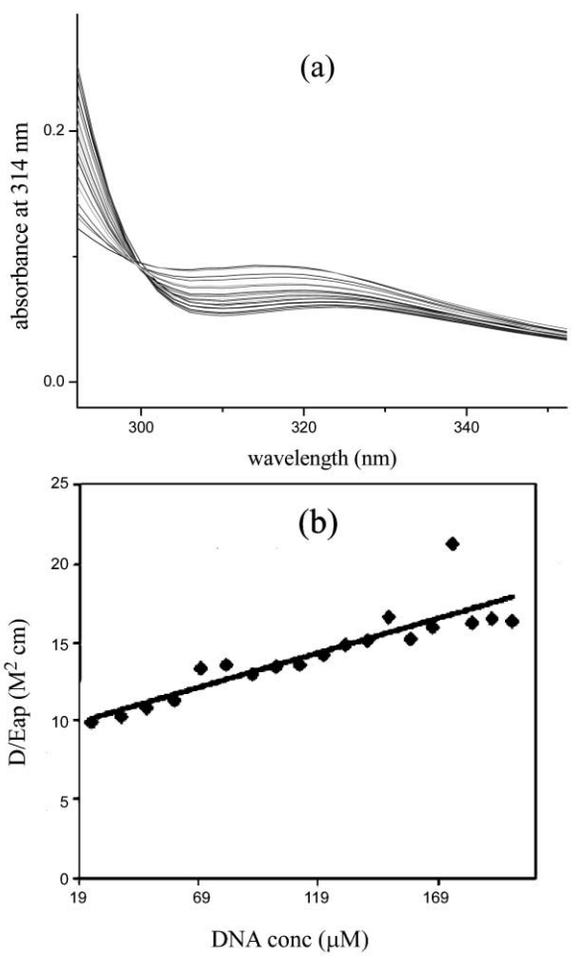


**Fig. 2** (a) UV spectrophotometric titration curves and (b) half-reciprocal plot for 1C2mac.

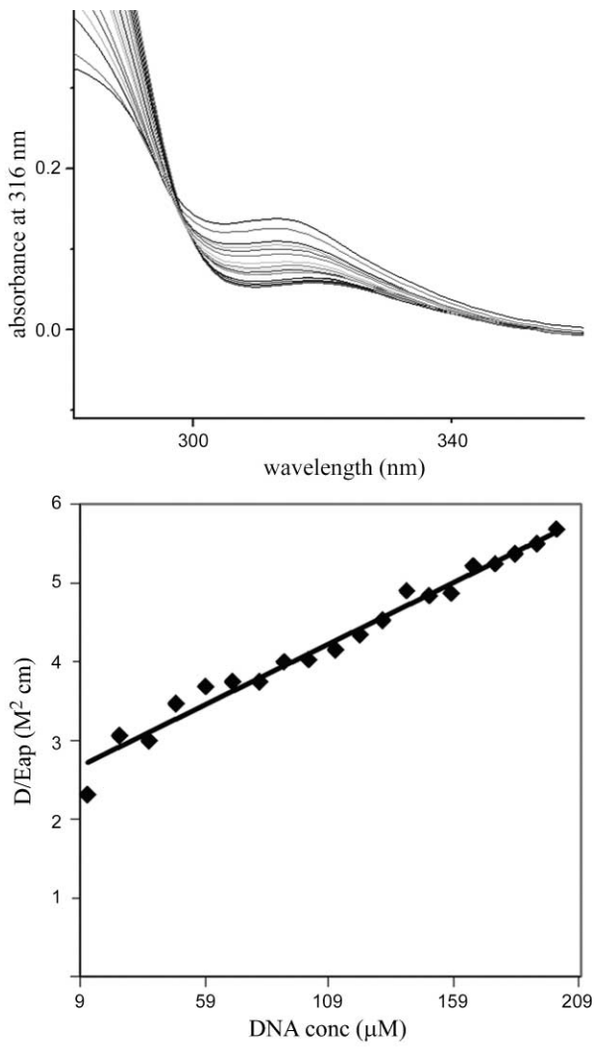


**Fig. 3** (a) UV spectrometric titration curves and (b) half-reciprocal plot for Cu–1C2mac.

mM). The apparent binding constants ($K_{ap}$) were determined from the half-reciprocal plots (Figs. 2(b) and 3(b)) and were found to be $4.7 \times 10^3$ $M^{-1}$ for 1C2mac and $6.2 \times 10^3$ $M^{-1}$ for Cu–1C2mac. These values, and the change on addition of $Cu^{2+}$, are comparable with those found by Kikuta *et al.*[12] who reported binding constants for an anthraquinone attached to the 12-membered macrocycle *via* a one-carbon chain (9,10-anthraquinon-2-yl)methyl-1,4,7,10-tetraazacyclododecane, $K_{ap}$

**Table 2** Concentrations and $R_t$ values (complexes per base pair) at which supercoiled DNA was unwound to an open-circular conformation

| Compound | Concentration/μM | $R_t$ |
|---|---|---|
| 1C2mac | 21 | 0.69 |
| Cu–1C2mac | 2 | 0.07 |
| 1C3mac | 4 | 0.13 |
| 2C3mac | 4 | 0.13 |
| Daunomycin | 5–10 | 0.17–0.34 |

$= 5.9 \times 10^3$ $M^{-1}$) and its $Cu^{2+}$ complex ($K_{ap} = 8.9 \times 10^3$ $M^{-1}$). The binding constant was three times greater for the $Zn^{2+}$ containing macrocycle ($K_{ap} = 2.8 \times 10^4$ $M^{-1}$), suggesting that the metal plays an important role in determining the affinity of the complex for DNA.

### Plasmid binding assays

The DNA binding of the cyclam/anthraquinone adducts and their metal complexes was compared by reacting them with plasmid DNA and separating the products using gel electrophoresis. The results are summarised in Table 2. Binding at the GpG and GpC sites was probed using the restriction enzymes *Bam*H1 and *Pvu*II which cleave at the 5′-**GG**ATCC-3′ and 5′-CA**GC**TG-3′ sequences, respectively.

Fig. 4(a) shows the gel for PBR322 DNA treated with 1C2mac. As the concentration of 1C2mac was increased, the supercoiled DNA became increasingly unwound as shown by a decrease in its mobility. The supercoiled DNA became open circular when the concentration of 1C2mac reached approximately 21 μM, representing an $R_t$ value of 0.69. After this point, it is difficult to determine with certainty which band of DNA corresponds to the nicked open circular form and which band corresponds to the unwound supercoiled form due to their proximity on the gel. One interpretation of the gel in this region is that the mobility of the unwound supercoiled DNA decreased further so that it is slightly less than that of the nicked open circular DNA while the mobility of the open circular nicked DNA increased slightly. Another interpretation is that the unwound supercoiled DNA recoiled in the opposite direction after this point leading to a slight increase in its mobility while the mobility of the nicked open circular DNA remained the same. The latter interpretation is more consistent with the behaviour of the DNA when exposed to 1C3mac and 2C3mac and with the effect of 1C2mac on linear DNA.

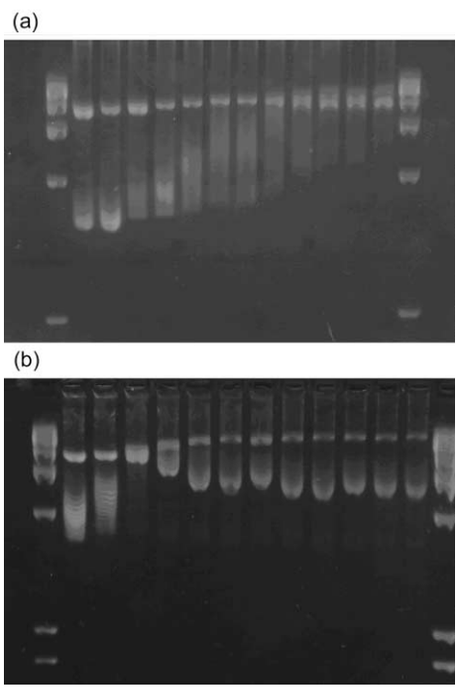


**Fig. 4** Gel electrophoresis patterns of PBR322 DNA treated with (a) 1C2mac and (b) 1C3mac. The lanes (from left to right) correspond to the marker, control-DNA only, then concentrations of 1, 4, 7, 11, 15, 18, 21, 25, 29, 32 and 36 μM of intercalator incubated with DNA, followed by the marker.

The results for 1C3mac (Fig. 4(b)) are remarkably different in that the supercoiled DNA becomes open circular when the concentration of 1C3mac reaches approximately 4 μM, four-fold lower than the concentration of 1C2mac needed to achieve maximum unwinding. After this point, the mobility of the supercoiled DNA increased until it tapered off at a concentration of 21 μM. The open circular nicked DNA decreased in mobility slightly with increasing 1C3mac concentration until 21 μM was reached, after which it tapered off. The gel electrophoresis pattern for 2C3mac treated DNA (ESI, † Fig. S2) shows similar results to those seen for 1C3mac in that the supercoiled DNA became open circular when the concentration of 2C3mac reached approximately 4 μM. After this point, the mobility of the supercoiled DNA increased until it tapered off at a 2C3mac concentration of 15 μM. The open circular nicked DNA decreased in mobility slightly with increasing 2C3mac concentration until 15 μM was reached.

Comparing the plasmid binding assays for an anthraquinone with an unmodified amine side chain (2C2, ESI, † Fig. S5) with those for the cyclam/anthraquinone adducts (Table 2) reveals that addition of the macrocycle has a strong influence on the binding of the intercalator. The anthraquinones by themselves produce very little change in the mobility or unwinding of the supercoiled DNA probably because of the high lability of the intercalation of the simple anthraquinones preventing any permanent unwinding of the DNA. In contrast, 1C2mac unwinds the supercoiled DNA and it becomes open circular at an $R_t$ of 0.69 indicating that the macrocycle is enhancing the binding of the anthraquinone. This enhanced binding could be due to hydrogen bonding associations between the macrocycle and the DNA and/or to the macrocycle being dipositively charged at neutral pH. Also possible is the presence of a cation within the cyclam, (*e.g.* $Cs^+$, $K^+$ and $Mg^{2+}$) which would also result in a charged species capable of binding electrostatically. Daunomycin, which is an excellent intercalator, fully unwinds the supercoiled DNA at lower concentrations ($R_t = 0.17$–$0.34$) than does 1C2mac ($R_t = 0.69$) which probably reflects differences in the strength of binding to the DNA. The 1C3mac and 2C3mac compounds (ESI, † Figs. S1 and S2) fully unwound the supercoiled DNA to become open circular at an $R_t$ of 0.13 indicating that these compounds are more efficient at unwinding the DNA than is 1C2mac. This is probably due to the longer chain length connecting the two moieties providing a macrocycle moiety better placed for interaction with the DNA phosphate backbone.

The addition of either *Bam*H1 (which cuts at a site containing GpG) or *Pvu*II (which cuts at a site containing GpC) restriction enzymes to supercoiled DNA results in restriction to linear DNA at all concentrations of 1C2mac, 1C3mac or 2C3mac (Fig. 5). This indicates that the cyclam/anthraquinone adducts do not inhibit the restriction of the DNA at either of these two sites. This may be due to the complex being present at the site, but not interfering with the restriction enzyme. However, given the strong stabilising interaction between the macrocycle and the DNA, it is more likely to be due to the complex binding at other sites. Daunomycin, similarly, causes no inhibition of the restriction by *Bam*H1 over the concentration range examined. However, at high concentrations, daunomycin inhibits some restriction by *Pvu*II (ESI, † Fig. S6) whereas there is no inhibition of restriction by *Pvu*II at high concentrations of any of the cyclam/anthraquinone adducts. This could be due to a greater binding strength of daunomycin or the targeting of the *Pvu*II site resulting in the inhibition of

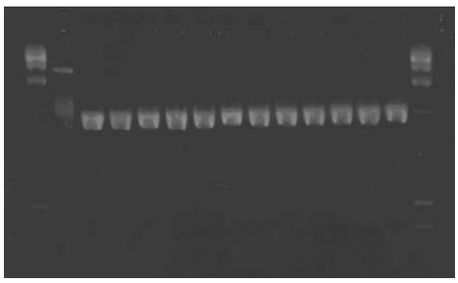

**Fig. 5** Gel electrophoresis pattern of PBR322 DNA treated with 1C2mac and *Bam*H1 restriction enzyme. The lanes (from left to right) correspond to the marker, control-DNA only, control-DNA and *Bam*H1 only, then concentrations of 1, 4, 7, 11, 15, 18, 21, 25, 29, 32 and 36 μM of 1C2mac incubated with DNA and *Bam*H1, followed by the marker.

restriction. There is also a possibility that the daunomycin interferes with *Pvu*II at high concentrations.

1C2mac causes no variation in the rate of migration of the linear DNA consistent with the effects on supercoiled DNA being almost entirely due to unwinding. 1C3 and 2C3 cause a slight decrease in mobility after the addition of 1 μM of complex until 21 μM of complex has been added, after which the decrease tapers off. This decrease is probably due to the positive charge on the macrocyclic moiety reducing the attraction to the electrode and/or to the increased size of the DNA adduct relative to the DNA alone.

Complexation of copper to the 1C2mac adduct ligand substantially modifies the binding of the complex (Fig. 6) as

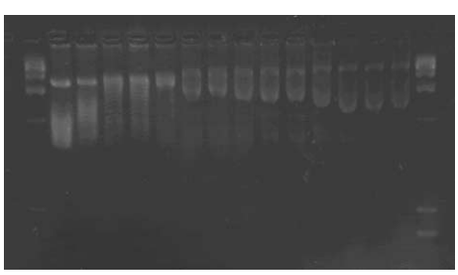

**Fig. 6** Gel electrophoresis pattern of PBR322 DNA treated with Cu–1C2mac. The lanes (from left to right) correspond to the marker, control-DNA only, then concentrations of 1, 2, 3, 4, 5, 6, 7, 8, 9, 10, 15, 20 and 25 μM of Cu–1C2mac incubated with DNA, followed by the marker.

indicated by the lower concentration required to fully unwind the supercoiled DNA (2 μM, $R_t = 0.07$). This may be due to the charge of the copper(II) complex, but there is also the possibility of nucleophilic sites on the DNA binding in the axial positions of the copper resulting in greatly increased binding and/or unwinding. Metal binding to DNA has been reported previously for $Zn^{2+}$ bound in a cyclen/anthraquinone ligand.[12] The addition of the restriction enzymes *Bam*H1 and *Pvu*II in the presence of Cu–1C2mac adduct resulted in the restriction of the DNA to its linear form over the full range of concentrations tested (Fig. 7). This indicates that the Cu–1C2mac complex does not inhibit restriction at these sites. However, Cu–1C2mac caused more unwinding than daunomycin, so it is possible that, even though Cu–1C2mac causes less inhibition of the PvuII digestion enzyme, that it binds more strongly at other sequences.

There was a slight decrease in the mobility of linear DNA up to a concentration of 10 μM of Cu–1C2mac ($R_t = 0.33$) probably due to the DNA becoming saturated with the complex. This contrasts with the effect of 1C2mac which causes no change in the mobility of linear DNA over the concentration range examined. This difference could be due to a combination of factors such as changes in the mass, charge or degree of unwinding of the DNA. The Cu–1C2mac complex

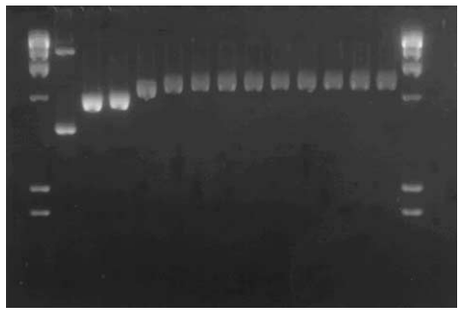

**Fig. 7** Gel electrophoresis pattern of PBR322 DNA treated with Cu–1C2mac and *Bam*H1 restriction enzyme. The lanes (from left to right) correspond to the marker, control-DNA only, control-DNA and *Bam*H1 only, then concentrations of 1, 5, 10, 15, 20, 25, 30, 35, 40, 45 and 50 μM of Cu–1C2mac incubated with DNA and *Bam*H1, followed by the marker.

may be less labile because of a stronger interaction with DNA resulting in the slower progress of the bulkier complex/DNA adduct through the electrophoresis gel. The 2+ charge of the copper within the macrocycle may also strengthen the interaction of the complex with DNA. However, it is notable that the UV-titrations gave similar values for the binding constants of 1C2mac and its copper complex. Therefore, the changes in mobility and unwinding are likely to be specific effects of the copper ion or the complex on these properties.

It is clear that adding a macrocyclic moiety (with or without a metal present) greatly enhances the binding of the intercalating moiety. There is significant disruption to the DNA arising from the combination of an intercalator uncoiling the DNA and a macrocyclic moiety reducing the intercalators lability and itself interacting with the DNA.

## Molecular modelling

Molecular modelling was used to investigate the interaction with DNA of the copper complexes of the anthraquinone: macrocycle adducts. The effect of the position of the side chain linking the anthraquinone to the macrocycle on interactions between the DNA and the macrocycle was examined by modelling the binding of 1C2mac and 2C2mac. Models were investigated with the long axis of the anthraquinone either perpendicular to the bases or parallel to them and with the macrocycle lying in either the minor groove or the major groove. In each case, only a single enantiomer was modelled because detailed investigation of the interactions between the macrocycle and the DNA are beyond the scope of the current study.

Fig. 8 shows Cu–1C2mac bound to DNA with the anthraquinone moiety intercalating from the major groove. For either orientation of the anthraquinone (parallel or perpendicular), the metal containing macrocycle can sit unhindered in the major or minor groove. Fig. S7† shows the overlap of the anthraquinone moiety of the cyclam/1-anthraquinone complexes with the pair of bases above and below the plane, with the anthraquinone in different orientations. When the 1-anthraquinone is inserted parallel to the DNA bases, slight rotation is required to accommodate the side chain and macrocyclic moiety in the minor groove (ESI,† Fig. S7(a)). The cyclam causes little steric hindrance when the side chain protrudes into the major groove (ESI,† Fig. S7(b)). When the 1-anthraquinone is inserted perpendicular to the DNA bases with the side chain in the minor groove (ESI,† Fig. S7(c)), it slides out into the minor groove to reduce the steric interactions with the DNA. When the side chain is placed in the major groove (ESI,† Fig. S7(d)), there is a rotation away from the perpendicular orientation to accommodate the side chain. There is significant overlap between the DNA bases and the anthraquinone when its long axis is parallel to the long axis of the DNA bases, but

**Table 3** Comparisons between the modelling fetures of the 1- and 2-anthraquinone:macrocycles

| Side chain position | Orientation compared to DNA bases | Groove | Energy/kJ mol$^{-1}$ | Cavity/Å | Unwinding angle/° |
|---|---|---|---|---|---|
| 1 | Perpendicular | Minor | −2799 | 6.7 | 19.5 |
| 1 | Perpendicular | Major | −2797 | 6.6 | 16.7 |
| 1 | Parallel | Minor | −2814 | 6.6 | 15.1 |
| 1 | Parallel | Major | −2787 | 6.8 | 16.4 |
| 2 | Perpendicular | Minor | −2799 | 6.9 | 10.9 |
| 2 | Perpendicular | Major | −2780 | 6.5 | 13.4 |
| 2 | Parallel | Minor | −2814 | 6.4 | 18.8 |
| 2 | Parallel | Major | −2796 | 6.4 | 21.5 |

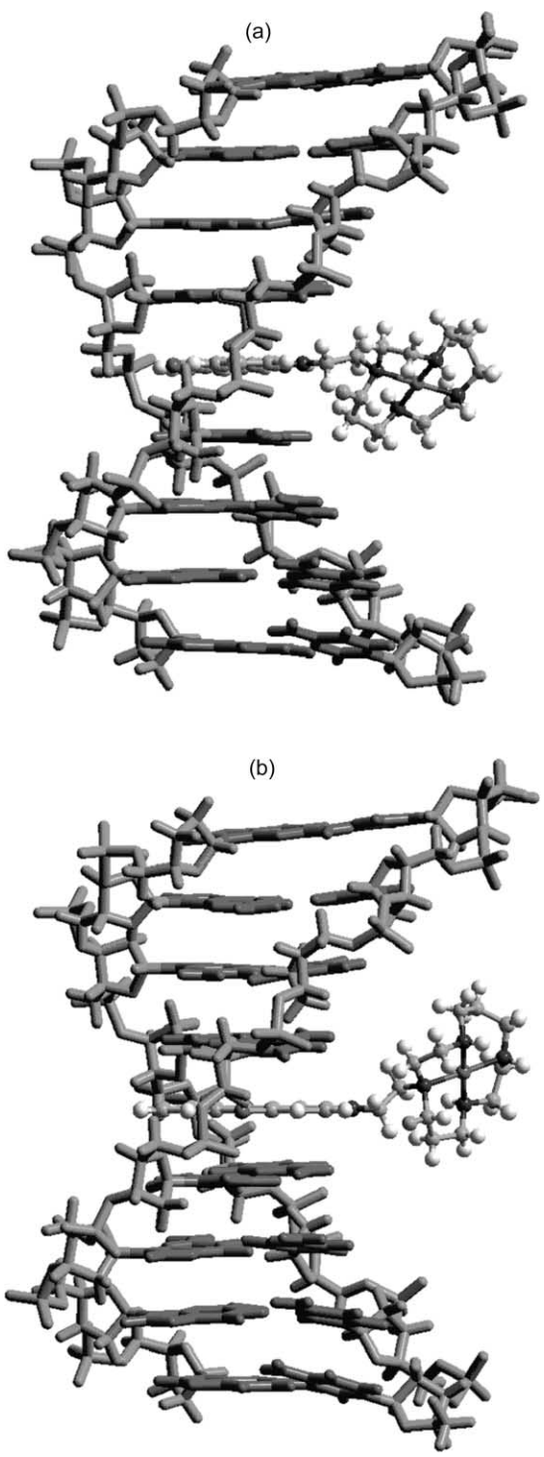


**Fig. 8** Molecular models of metal-1C2mac with the anthraquinone moiety intercalated within the DNA in either (a) the parallel position or (b) the perpendicular position, with the metal-macrocycle sitting out in the major groove.

there is less overlap when it is perpendicular to the DNA base axis (ESI,† Fig. S7(c) and (d)).

Fig. S8† shows the overlap of the anthraquinone moiety of the cyclam/2-anthraquinone complex, Cu–2C2mac, with the pair of bases above and below it. When the 2-anthraquinone is inserted perpendicular to the DNA bases, with the side chain in either the major or minor groove (ESI,† Fig. S8(a) and (b)), there is no change needed in the orientation to accommodate the side chain and the macrocycle. When the 2-anthraquinone is inserted parallel to the DNA bases with the side chain in the minor groove (ESI,† Fig. S8(c)), the anthraquinone shifts sideways to reduce the steric interactions between the DNA and the side chain. When the side chain is placed in the major groove (ESI,† Fig. S8(d)), only slight rotation away from the perpendicular orientation is necessary to accommodate this side chain. There is significant overlap between the DNA bases and the anthraquinone when the long axis of the 2-anthraquinone is orientated parallel to the long axis of the DNA bases, but there is less overlap when it sits in a position perpendicular to the long axis of the DNA bases (ESI,† Fig. S8(c) and (d)).

All of the intercalative modes modelled, regardless of the position or length of the side chains or the orientation of the anthraquinone within the DNA, appear to be viable due to the minimal disturbance to the DNA stacking and the significant amount of overlap between the DNA bases and the anthraquinone rings. Some of the features of the models, including energies, size of the cavity created with intercalation and the amount of DNA unwinding are listed in Table 3. The energies are similar and cannot be used to distinguish between the different binding orientations. The cavity sizes are all similar and are in accord with reported values for other intercalating moieties of approximately 6.8 Å.[33] The unwinding angles vary between 13.4 and 21.5 °, with no systematic trends evident.

The models of the Cu–1C2mac with the 1-anthraquinone moiety intercalated in an 8-mer showed that the complex was better accommodated when the 1-anthraquinone was in the parallel position (especially when in the major groove) with little steric hindrance between the complex and the DNA. Even though the position of the side chain was better accommodated in the major groove due to the larger space available, the electrostatic interactions between the cationic groups in the side chains of the intercalators and the negative electrostatic potential of the minor groove[34] as well as the possibility of close van der Waals contacts within the minor groove are expected to favour binding from this groove. The anthraquinones with the side chains in the 2-position were easily accommodated in the DNA either parallel or perpendicular to the DNA bases.

It is clear from the models that the chain length does not influence the ability of the cyclam/anthraquinone to intercalate. Therefore, the effects of chain length on the plasmid binding properties described above, are probably indicative of specific interactions between the macrocycle and the DNA that are facilitated by the longer linker.

## Conclusions

The anthraquinone/cyclam adducts and their metal complexes represent exciting new compounds that have excellent DNA binding properties. There is the potential to produce many variations of this adduct by varying such things as the intercalating moiety, the nature of the metal ion, macrocycle size, composition and/or donor atom types, side chain position, length and/or composition as well as the number and/or positions of the intercalators on the macrocycle. These can all be varied to optimise the adduct properties and achieve desired behaviours.

## References


1 S. Jurisson, D. Berning, W. Jia and D. Ma, *Chem. Rev.*, 1993, **93**, 1137.
2 E. Kimura and E. Kikuta, *J. Biol. Inorg. Chem.*, 2000, **5**, 139.
3 E. Kimura, T. Ikeda and M. Shionoya, *Pure Appl. Chem.*, 1997, **69**, 2187.
4 D. Gibson, N. Mansur and K. F. Gean, *J. Inorg. Biochem.*, 1995, **58**, 79.
5 J. Whittaker, W. D. McFadyen, G. Wickham, L. P. G. Wakelin and V. Murray, *Nucleic Acids Res.*, 1998, **26**, 3933.
6 L. C. Perrin, P. D. Prenzler, C. Cullinane, D. R. Phillips, W. A. Denny and W. D. McFadyen, *J. Inorg. Biochem.*, 2000, **81**, 111.
7 M. Shionoya, T. Ikeda, E. Kimura and M. Shiro, *J. Am. Chem. Soc.*, 1994, **116**, 3848.
8 E. Kimura, M. Kikuchi, H. Kitamura and T. Koike, *Chem. Eur. J.*, 1999, **5**, 3113.
9 E. Kikuta, M. Murata, N. Katsube, T. Koike and E. Kimura, *J. Am. Chem. Soc.*, 1999, **121**, 5426.
10 S. Aoki and E. Kimura, *J. Am. Chem. Soc.*, 2000, **122**, 4542.
11 E. Kimura, H. Kitamura, K. Ohtani and T. Loike, *J. Am. Chem. Soc.*, 2000, **122**, 4668.
12 E. Kikuta, R. Matsubara, N. Katsube, T. Koike and E. Kimura, *J. Inorg. Biochem.*, 2000, **82**, 239.
13 G. M. Sheldrick, SADABS. Empirical absorption correction program for area detector data, 1996.
14 Bruker SMART, SAINT, XPREP, Bruker Analytical X-ray Instruments, Inc., Madison, WI, USA, 1995.
15 G. M. Sheldrick, in Crystallographic Computing 3 ed. G. M. Sheldrick, C. Kruger and R. Goddard, Oxford University Press, 1986.
16 teXsan, Version 1.8 ed., Molecular Structure Corporation, The Woodlands, TX, 1992–1997.
17 *International Tables for X-ray Crystallography*, Kynoch Press, Birmingham, vol. 4, 1974.
18 J. A. Ibers and W. C. Hamilton, *Acta Crystallogr.*, 1964, **17**, 781.
19 D. C. Creagh and W. J. McAuley, *International Tables for Crystallography, Vol. C, Table 4.2.6.8*, Kluwer Academic Publishers, Boston, MA, 1992.
20 D. C. Creagh and J. H. Hubbell, *International Tables for Crystallography, Vol. C, Table 4.2.4.3*, Kluwer Academic Publishers, Boston, MA, 1992.
21 C. K. Johnson, ORTEP-II, A FORTRAN Thermal-Ellipsoid Plot Program, Oak Ridge National Laboratory, Oak Ridge, TN, 1976.
22 R. D. Wells, J. E. Larson, R. C. Grant, B. E. Shortle and C. R. Cantor, *J. Mol. Biol.*, 1970, **54**, 465.
23 S. Arounaguiri and B. G. Maiya, *Inorg. Chem.*, 1996, **35**, 4267.
24 J. A. Broomhead, L. M. Rendina and L. K. Webster, *J. Inorg. Biochem.*, 1993, **49**, 221.
25 T. M. Jones-Wilson, K. A. Deal, C. J. Anderson, D. W. McCarthy, Z. Kovacs, R. J. Motekaitis, A. D. Sherry, A. E. Martell and M. J. Welch, *Nucl. Med. Biol.*, 1998, **25**, 523.
26 HyperCube, in HYPERCHEM, Release 4.5 for Windows, 1995.
27 T. W. Hambley, in MOMECSG, Programme for Strain Energy Minimisation, 1996.
28 M. Engeser, L. Fabbrizzi, M. Licchelli and D. Sacchi, *Chem. Commun.*, 1999, 1191.
29 J. Katzhendler, K.-F. Gean, G. Bar-ad, Z. Tashma, R. Ben-Shoshan, I. Ringel, U. Bachrach and A. Ramu, *Eur. J. Med. Chem.*, 1989, **24**, 23.
30 D. Gibson, I. Binyamin, M. Haj, I. Ringel, A. Ramu and J. Katzhendler, *Eur. J. Med. Chem.*, 1997, **32**, 823.
31 M. J. Scott and R. H. Holm, *J. Am. Chem. Soc.*, 1994, **116**, 11357.
32 P. Almond, S. D. I. Cutbush, S. A. Islam, R. Kuroda and S. Neidle, *Acta Crystallogr., Sect. C*, 1983, **39**, 627.
33 H. M. Berman and P. R. Young, *Annu. Rev. Biophys. Bioeng.*, 1981, **10**, 87.
34 G. M. Blackburn and M. J. Gait, *Nucleic Acids in Chemistry and Biology*, IRL Press at Oxford University Press, Oxford, 1990.